Liquid Crystals
Publication details, including instructions for authors and subscription information:
http://www.informaworld.com/smpp/title~content=t713926090

Dynamics of nematic point defects in a capillary with tilted boundary conditions

J. Bajc; G. Guidone Peroli; E. G. Virga; S. Žumer

Online publication date: 11 November 2010

To cite this Article Bajc, J. , Peroli, G. Guidone , Virga, E. G. and Žumer, S.(2002) 'Dynamics of nematic point defects in a capillary with tilted boundary conditions', Liquid Crystals, 29: 2, 213 — 219
To link to this Article: DOI: 10.1080/02678290110093787
URL: http://dx.doi.org/10.1080/02678290110093787

LIQUID CRYSTALS, 2002, VOL. 29, NO. 2, 213–219

Dynamics of nematic point defects in a capillary with tilted boundary conditions

J. BAJC*, G. GUIDONE PEROLI†, E. G. VIRGA† and S. ŽUMER

Department of Physics, University of Ljubljana, Jadranska 19, SI-1000 Ljubljana, Slovenia

†Dipartimento di Matematica, Istituto Nazionale di Fisica della Materia, via Ferrata 1, I-27100 Pavia, Italy

(*Received 1 April 2001; accepted 1 August 2001*)

The motion of a single point defect in a cylindrical cavity filled with a nematic liquid crystal is described by solving numerically the simplified equations of nematodynamics. Perfect homeotropic anchoring for the director on the lateral boundary would result in the creation of domains with equal elastic energy, escaped upwards or downwards along the cavity axis and separated by point defects of strength ± 1. Defects do not move as long as they are sufficiently far apart. However, small deviations from homeotropic anchoring remove this degeneracy and the energetically favourable domains start to expand at the expense of the others, thus setting the defects in motion along the tube. We present a new numerical approach, which neglects the backflow, for studying the influence of both the pretilt and the elastic anisotropy ($K_{33} \neq K_{11}$) on the motion of a defect. We show how even very small pretilt angles ($\sim 1^\circ$) result in speeds observed in experiments. For a moderate elastic anisotropy, the velocity of a $+1$ defect equals the velocity of a -1 defect, whereas for $K_{33} \gg K_{11}$ a $+1$ defect moves faster than a -1 defect. For small pretilts we confirm a good qualitative agreement with an existing analytical approach, which proves inaccurate for large pretilts.

1. Introduction

Recently, and in particular in connection with coarsening dynamics, the motion of defects in condensed matter is again attracting much interest, both experimentally and theoretically; see, for example, [1–3]. Although the first experiments with defects in nematic liquid crystals confined to cylindrical cavities date back to the 1970s, the theoretical interpretation of the experimental results is still a matter of dispute. Steady motion was reported for defects connected in pairs by strings [3–5] and for a single defect separating two domains with different free energy densities. This latter case, realized in a capillary with pretilted anchoring, was first reported and qualitatively described by Guidone Peroli *et al.* [6, 7]. The motion of a single defect driven by slightly tilted anchoring conditions on the lateral boundary of a cylindrical tube represents one of the simplest dynamical phenomena involving defects in liquid crystals. It serves as a test for different theoretical approaches, whose outcomes could be compared with the available experimental data.

In cylindrical cavities with homeotropic anchoring, the known equilibrium structures for the director field, namely, planar radial, planar polar, and escaped, can all be stable [8]. When the radius R of the tube is large enough ($R \gtrsim 1\,\mu$m) the escaped structure is the only stable one. Director fields escaped either upwards or downwards along the tube axis are energetically equivalent, and so domains with opposite escapes can appear, each separated from the adjacent one by a point defect with topological charge s of strength 1 and alternating sign.

The anchoring on the lateral boundary of a capillary tube can, however, fail to be homeotropic. Here we imagine the director to be tilted relative to the boundary normal, everywhere in one and the same direction along the axis of the tube. It might be expected that the resulting director configurations would be only slightly altered, especially when the *pretilt* angle φ_0 is sufficiently small. Figure 1, however, illustrates that this is not the case: upwards and downwards escapes now fail to be symmetric, thus removing the degeneracy of the homeotropic anchoring. In the presence of a defect, this lack of symmetry is enough to produce a dramatic change: the two tilted configurations cannot be at equilibrium, because the domains with opposite escapes now store different energies, the one fluted in the same direction as the boundary director being less distorted than the other, as sketched in figure 1 for a $+1$ and a -1 defect. One domain then expands at the expense of the other, thus pulling the point defect in the domain wall between

*Author for correspondence; e-mail: jure.bajc@gov.si

Liquid Crystals ISSN 0267-8292 print/ISSN 1366-5855 online © 2002 Taylor & Francis Ltd
http://www.tandf.co.uk/journals
DOI: 10.1080/02678290110093787

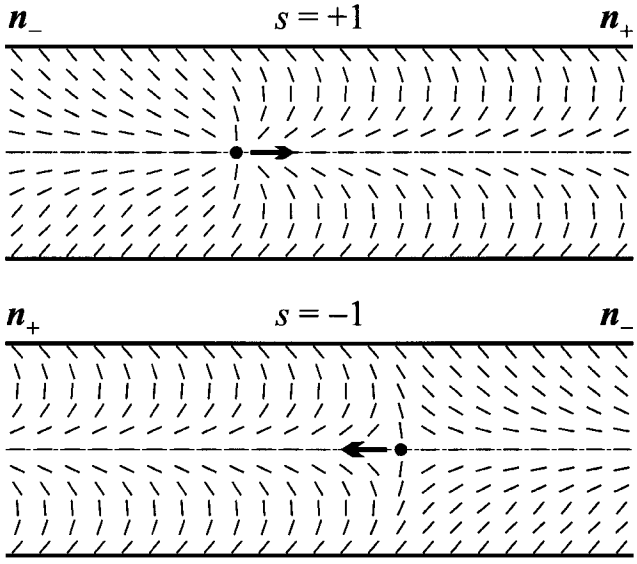

Figure 1. Schematic representation of the fields $\mathbf{n}_-$ and $\mathbf{n}_+$. The topological charges are $s = +1$ (top) and $s = -1$ (bottom). The arrow indicates the direction of motion.

them. Here we study in detail the motion of a single point defect along the axis of a cylindrical tube, a phenomenon first predicted and approximately described in [6], to explain qualitatively some experimental data indicating a constant speed in the early stages of the coalescence of two defects [9].

In § 2, we give a concise theoretical account of the continuum theory for nematic liquid crystals. We calculate the torques acting on the nematic director, and show how the nematodynamics, which is dominated by friction, can be described either as a balance between viscous and elastic torques or as the dissipation of elastic energy during the rearrangement of the director in time. We briefly recall a simple analytical model for the evolution of the director field around a point defect [6]. In § 3, this process is simulated numerically by use of a new adapted relaxation method to describe the motion of the defect and to explore the role played by the elastic anisotropy of the material. In § 4, we discuss our results and compare them with previous theoretical outcomes and experimental data. The paper is closed by a discussion in § 5 on further applications of the proposed method and its possible improvement.

2. Theory

The molecules of a nematogenic material are typically elongated in one direction. On average, the long molecular axes tend to orient parallel to one another, and their average direction is described by a director field $\mathbf{n}$. This field represents a mapping onto the unit sphere S^2. We say that a defect occurs wherever the map $\mathbf{n}$ is discontinuous. The elastic free energy stored in a region $\mathcal{B}$ was given the following form by Oseen and Frank:

$$\begin{aligned}\mathcal{F}[\mathbf{n}] = \frac{1}{2}\int_{\mathcal{B}} \{&K_{11}(\operatorname{div}\mathbf{n})^2 \\ &+ K_{22}(\mathbf{n}\cdot\operatorname{curl}\mathbf{n})^2 + K_{33}|\mathbf{n}\wedge\operatorname{curl}\mathbf{n}|^2 \\ &+ (K_{22}+K_{24})[\operatorname{tr}(\Delta\mathbf{n})^2 - (\operatorname{div}\mathbf{n})^2]\}\,\mathrm{d}V \end{aligned} \quad (1)$$

where the moduli K_{11}, K_{22}, K_{33}, and K_{24} are the splay, twist, bend, and saddle-splay elastic constants, respectively. Equation (1) reduces to a far simpler form if we set $K_{11} = K_{22} = K_{33} = K$ and $K_{24} = 0$, that is,

$$\mathcal{F}[\mathbf{n}] = \frac{K}{2}\int_{\mathcal{B}} |\nabla\mathbf{n}|^2\,\mathrm{d}V \quad (2)$$

which is known as the *one-constant approximation* to $\mathcal{F}$. The equilibrium equation for (1) can be written as

$$\mathbf{H} := \mathbf{h} - (\mathbf{n}\cdot\mathbf{h})\mathbf{n} = 0; \quad \mathbf{h} := -\frac{\partial f}{\partial \mathbf{n}} + \operatorname{div}\left(\frac{\partial f}{\partial \nabla\mathbf{n}}\right) \quad (3)$$

where f is the integrand on the right-hand side of (1) and $\mathbf{h}$ is the *molecular field* (cf. p. 107 of [10]). If $\mathcal{B}$ is an infinite cylinder with radius R that enforces homeotropic anchoring on its lateral boundary, the solutions of equation (3) are the well-known *escaped* fields [11, 12]. In the one-constant approximation (2), the analytical form of these fields in the frame $(\mathbf{e}_r, \mathbf{e}_\vartheta, \mathbf{e}_z)$ of cylindrical coordinates is

$$\begin{aligned}&\mathbf{n}_\pm = \cos\varphi_\pm\,\mathbf{e}_r + \sin\varphi_\pm\,\mathbf{e}_z \quad \text{with} \\ &\varphi_\pm(r) = \pm\left[\frac{\pi}{2} - 2\arctan\left(\frac{r}{R}\right)\right]\end{aligned} \quad (4)$$

where one sign or the other applies according to whether the director field escapes upwards ($\mathbf{n}_+$) or downwards ($\mathbf{n}_-$) along $\mathbf{e}_z$. By symmetry, both these fields store the same elastic energy per unit length of the cylinder.

The simplest escaped field that fails to be uniform in z has a single defect with topological charge s either $+1$ or -1, placed somewhere along the axis $r = 0$. Changing the position of the defect, that is, moving the domain wall, obviously does not change the total free energy, and so no force acts on the defect. To allow it to move spontaneously, this symmetry must somehow be broken. It was conjectured that the filling of the capillary might determine a favoured direction and produce a slight deviation from the homeotropic anchoring [6]. The degeneracy of the homeotropic anchoring is thus removed and one escaped domain is more energetic than the other. The less energetic domain tends to expand at the expense of the other, an effective force on the defect then appears and sets it in motion.

The time evolution of non-equilibrium nematic configurations is well described by the equations of nematodynamics [13, 14]. Away from equilibrium, **H** is different from zero. It represents the generalized elastic force acting on the director **n**: when this evolves towards less energetic configurations, some kind of friction is likely to be involved, as Landau and Khalatnikov pointed out in general nearly 50 years ago [15]. In the case of nematics, the appropriate friction is quite complicated and a complete description involves five independent viscosity coefficients coupling different reorientation modes with the hydrodynamic flow; see [13, 14]. For simplicity, in the following we neglect completely the *backflow*, that is, the flow induced by the director motion: thus, only the *rotational viscosity* γ_1, responsible for the friction on the director reorientation, will be taken into account. Although the effects of the back-flow on the motion of a point defect seems to be so subtle as to depend on the sign of the defect's topological charge [16] (a view also supported by some experimental evidence [5]), we shall here neglect them because no technique (either analytical or numerical) is yet available to include them. In this respect our study is still preliminary. On the other hand, it is more justifiable to neglect the inertial terms, because nematodynamics proves to be completely dominated by friction [10]. Thus, the balance of the generalized elastic and viscous forces results in the equation of motion

$$\gamma_1 \dot{\mathbf{n}} = \mathbf{H} \tag{5}$$

where a superimposed dot denotes the material time derivative. Upon assuming that **n** is an axisymmetric field even in the presence of defects (see figure 1), that is,

$$\mathbf{n} = \cos\varphi(t, r, z)\mathbf{e}_r + \sin\varphi(t, r, z)\mathbf{e}_z \tag{6}$$

equation (5) becomes

$$\begin{aligned}\gamma_1\varphi_t = {} & (K_{11}\sin^2\varphi + K_{33}\cos^2\varphi)\frac{1}{r}(r\varphi_r)_r \\ & + (K_{11}\cos^2\varphi + K_{33}\sin^2\varphi)\varphi_{zz} \\ & - (K_{11} - K_{33})\cos(2\varphi)\varphi_r\varphi_z + \sin\varphi\cos\varphi \\ & \times\left[\frac{K_{11}}{r^2} + (K_{11} - K_{33})\left(\varphi_r^2 - \frac{\varphi_z}{r} - 2\varphi_{rz} - \varphi_z^2\right)\right]\end{aligned} \tag{7}$$

where the subscripts t, r, and z denote partial derivatives with respect to the corresponding variables. Equation (5) embodies the balance between viscous and elastic torques acting on the director; as shown in [17], it can be derived from a dissipation principle (see [18] for a general method also applicable to fluids with more complex microstructures). In the absence of backflow and when the molecular kinetic energy is neglected, the balance of energy requires that the rate of change in the elastic free energy balances the viscous dissipation $\mathscr{D}$:

$$\dot{\mathscr{F}} + \mathscr{D} = 0. \tag{8}$$

When **n** is the axisymmetric field (6), $\mathscr{D}$ simply reduces to

$$\mathscr{D} = \gamma_1 \int_{\mathscr{B}} \varphi_t^2 \, \mathrm{d}V. \tag{9}$$

It is shown in [17] that expressions (8) and (5) agree.

The motion of a single defect along the axis of a capillary tube due to a prescribed pretilt on the lateral boundary has been studied qualitatively and explained by an analytical model in [6]. The complete mathematical description of the model can be found in [7, 19, 20]. Since our main objective here is to compare the outcomes of this model and those of a numerical approach to the same problem, we only briefly recall the basic ideas and the results of the analytical model. Solving explicitly the dynamical equation (7) is avoided by computing both the time rate $\dot{\mathscr{F}}$ of the elastic free energy and the dissipation $\mathscr{D}$ as functions of the speed v of the defect for a *frozen* director field around it. This director field is determined by solving an equilibrium problem. Essentially, one mimics the director around a defect with a $+1$ or -1 topological charge by minimizing the elastic free energy within a restricted class of admissible fields, all bearing a defect in a prescribed position. To within an non-essential additive constant, the energy stored in a cylinder enclosing a $+1$ defect turns out to be [6]

$$\mathscr{F} = 4\pi K \sin\varphi_0 z \tag{10}$$

where z is the position of the defect along the cylinder axis. One then imagines that the defect is free to move along the capillary axis, dragging along the static director field without distorting it. Knowing explicitly this field allows one to compute the dissipation $\mathscr{D}$ in equation (9) as a function of the defect velocity $v := \dot{z}$:

$$\mathscr{D} = \pi\gamma_1\pi^{1/2}R\cos\varphi_0\{[A(-\varphi_0)]^{1/2} + [A(\varphi_0)]^{1/2}\}v^2 \tag{11}$$

where R is the radius of the capillary and A is defined as

$$\begin{aligned}A(\varphi_0) := {} & \frac{1 + \sin\varphi_0}{1 - \sin\varphi_0}[2\ln 2 - 1 - 2\ln(1 + \sin\varphi_0) \\ & + \sin\varphi_0].\end{aligned} \tag{12}$$

The reader interested in more details about the computations leading to equation (11) will find them in [20]. Here it suffices to remark that by combining equations (11), (10), and (8) the velocity of a single

defect can be given the following form:

$$v = \frac{4}{\pi^{1/2}} \left\{ \frac{\tan \varphi_0}{[A(-\varphi_0)]^{1/2} + [A(\varphi_0)]^{1/2}} \right\} \frac{K}{\gamma_1 R}. \quad (13)$$

A natural measure for the velocity v is the ratio $K/(\gamma_1 R)$, which is inversely proportional to the radius of the tube: thus, defects move faster in smaller tubes.

Equation (13) shows that in a tube with tilted anchoring a single defect moves with a constant velocity which depends on the material constants of the liquid crystal and the pretilt angle φ_0. For small values of φ_0 this velocity is proportional to φ_0. The velocity v thus vanishes when $\varphi_0 = 0$, confirming that a defect does not move when the anchoring is homeotropic. To study the motion of defects in a more quantitative way that also takes into account non-equilibrium structures, we now turn to a numerical simulation.

3. Numerical approach

In contrast with the analytical approach, the numerical modelling of defect dynamics involves the full time evolution of the director field, which requires solving equation (7). In this section we briefly describe how this can actually be carried out.

The numerical computation is performed on a finite segment of the tube. When assigning the length of this segment, two opposite requirements must be satisfied: it should be sufficiently short to reduce the computational time, and sufficiently long to reduce the influence of the end-caps. To satisfy both requirements, equation (7) is solved in a rectangular non-uniform mesh, denser near the defect than farther away (see figure 2). To solve (7) we also need to impose the appropriate boundary conditions at the ends of the computational segment, which are not particularly obvious. We select them so as to match the equilibrium escaped structure that agrees with the boundary condition on the lateral wall and the appropriate escape direction. Both equilibrium structures (escapes upwards and downwards) are obtained by solving equation (7) for a given φ_0 on the lateral wall and only a radially dependent director, $\varphi = \varphi(r)$. The computational segment must thus be chosen to be long enough also to allow the director field to adjust to the escaped structure at both ends. It turns out that for modest pretilts and small elastic anisotropies, the director field relaxes to a nearly undistorted escaped configuration over the distance $2R$. A segment with length $6R$ having a single defect near the centre should thus suffice.

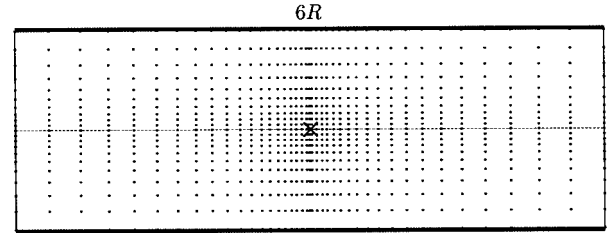

Figure 2. A non-uniform mesh to solve equation (7) with finite differences. The length of the computational segment is $6R$. The mesh shown here has 10×40 points in the $r \times z$ directions, whereas the one actually employed had 40×150 points.

Special care must be taken not to violate the head–tail symmetry of the nematic director in calculating the derivatives of φ, especially near defects where φ changes rapidly. If, for example, the difference $\Delta\varphi$ at two neighbouring mesh-points exceeds $\pi/2$, one would then argue that the actual difference is not $\Delta\varphi$, but $\Delta\varphi - \pi$, because the head–tail symmetry is thus preserved, while the director field exhibits less elastic energy along with smaller derivatives. It transpires that for sufficiently dense meshes the head–tail symmetry of regular director fields would not be violated even if the director field were treated as a regular vector field. On the contrary, when defects are present no mesh could possibly prevent this symmetry from being broken, no matter how dense. In the case under study the defect is located on the tube axis, but in general it can be anywhere between two neighbouring mesh-points. Derivatives of φ with respect to the radial coordinate are not critical even in the vicinity of the defect, because the changes of φ in the radial direction are smooth enough. Only the derivatives of φ with respect to the axial coordinate at the nearest mesh-points away from the cylinder axis might not be appropriately computed because of a spurious violation of the head–tail symmetry. Thus, for these mesh points, the director reorientation is calculated by also taking into account the surrounding points.

In the case of conical boundary conditions with only a defect, we developed a new method. Since by the above analysis the driving force is expected to be constant, it is natural to assume that the defect (together with the domain wall around it) soon reaches a steady asymptotic velocity. Practically, this means that the picture would not change, if the *camera*, so to say, were moving along the tube with the velocity of the defect. Numerical implementations of this idea would be relatively simple, if only the position of the defect could be determined accurately enough.

A certain initial director configuration is set forth with the defect placed somewhere in the middle of a chosen mesh-cell. Since we are deriving the steady asymptotic velocity solution, almost any initial structure surrounding the appropriate point defect, and satisfying the boundary conditions, is acceptable; for less realistic initial structures it will only take more iterations to reach the same final

quasi-stationary state. Then, φ_t is computed and values of φ in the entire mesh are changed in a small time step Δt. So the defect moves by Δz. After a number of steps it would approach the boundary of the mesh-cell, thus making it difficult to compute the derivatives of φ. To keep the defect inside the mesh-cell, the entire texture is shifted by $-\Delta z$. Numerically, this is done by a simple linear interpolation of φ from the closest mesh-points. This procedure yields a steady state when Δz fails to change at each step. In other words, the camera is then following a moving defect at precisely its velocity $v = \Delta z/\Delta t$. If the time steps are small enough, the defect remains near the centre of the mesh-cell and the numerical accuracy is expected to be improved.

For the above method it is crucial to determine the position of the defect as accurately as possible. The basic assumption behind the locating algorithm is a known director field in the immediate vicinity of a moving defect. We assume that even if a defect is moving at a considerable speed, the elastic forces prevail in its vicinity, and so in case of equal splay (K_{11}) and bend (K_{33}) elastic constants, the director fields with $s = \pm 1$ (also called the *radial* and *hyperbolic hedgehogs*, respectively) are locally described by the functions

$$\varphi_{\pm} = \pm \arctan\left(\frac{z}{r}\right). \tag{14}$$

In the numerical algorithm, the director field calculated in the vicinity of the defect is compared with the one modelled by (14). The putative position of the defect is varied while searching for the minimal difference between modelled and computed director fields. To keep this procedure to a minimum only the nearest mesh-points are taken into account (see figure 3). Since, by symmetry, the orientation of the director on the tube axis can only be parallel to the axis, two off-axis mesh-points alone are considered to locate the defect.

This algorithm is only reliable for cylinder radii much larger than the defect core and moderate pretilts, when the director field is likely to retain its equilibrium form in the vicinity of the defect. Although a denser mesh could improve the stability of the method, this would not solve the localization problem. High velocities result in deviations from the static solution at the very core of the defect [21], thus making it appropriate to resort to asymmetric hedgehogs or even to a variable scalar order parameter as well.

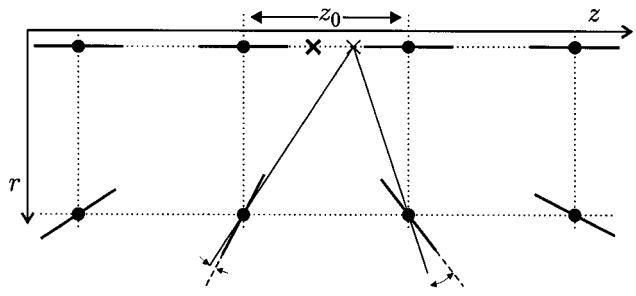

Figure 3. The point defect is located by comparing the radial hedgehog and the director field computed numerically in the vicinity of the tube axis.

4. Results

The numerical simulation for small pretilts in the one-constant approximation shows the expected dependence on the pretilt φ_0 (see figure 4). While the qualitative behaviour is the same for both approaches, the analytical velocity is approximately 40% less than the numerical one for pretilts below 20°. This difference can be explained by a simple argument. While the force acting on the defect is approximately the same in both models, as it arises simply from the lack of symmetry between the opposite escapes, the energy dissipated in the motion is clearly overestimated in the analytical approach, for which the director deformation around the defect is *stiffer* than for the numerical approach, as it is more constrained. Thus, equation (8), which holds for both approaches, qualitatively justifies the difference in the two estimates for the defect velocity. Moreover, the comparison between the elastic free energies for small pretilts (see figure 5) is also in a quantitative agreement with the above considerations. For a tube segment of length $6R$ with a defect in the centre, the energy that exceeds $12\pi KR$ is associated with the defect [20]. For small pretilts, the ratio between the free energies associated with the defect in the analytical and in the numerical approach is almost inversely proportional to the corresponding ratio of the velocities (figures 4 and 5). Thus, for small pretilts, the discrepancy between the two approaches is simply due to a more or less adequate

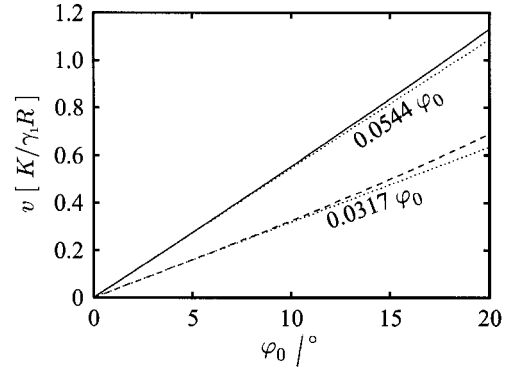

Figure 4. Velocity of a single defect as a function of the pretilt angle in the range $0 < \varphi_0 < 20°$. Solid and dashed lines refer to the numerical and analytical approaches, respectively. The linear approximation is indicated by a dotted line in both cases.

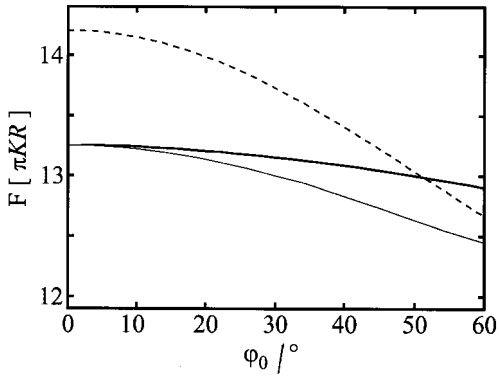

Figure 5. Total free energy in a tube segment around a moving point defect. The thick solid line and the dashed line refer to the numerical and analytical approaches, respectively. The hypothetical free energy stored around an artificially fixed defect is denoted by a thin solid line.

estimate of the energy of the defect. In other words, a defect that keeps more energy dissipates less and moves more slowly.

Further inspection of the elastic free energy shows that the validity of this criterion cannot be extended to larger values of the pretilt angle φ_0, as is clear from figure 5 for $\varphi_0 > 50°$, when the numerical elastic free energy becomes larger than the analytical one. We take this angle as the limit for the pretilt above which both the analytical and the numerical models are likely to break down. There are indeed several reasons why this should be the case. As shown in [20], the constrained structure that in the analytical model connects the defect to the escaped field $\mathbf{n}_+$ extends indefinitely along the capillary axis as $\varphi_0 \to 90°$. In particular, it reaches one end of the computational segment of length $6R$ when $\varphi_0 \simeq 86°$, which is the root of the equation

$$[A(-\varphi_0)\pi]^{1/2} = 3\cos\varphi_0. \qquad (15)$$

Then the total free energy stored in the segment is $\mathcal{F} \simeq 12\pi KR$. For $\varphi_0 > 86°$ the analytic solution would fail to obey the strong boundary conditions imposed by the numerical method. These, in turn, are likely to keep the defect away from its natural evolution for large values of the pretilt, when they become less realistic, as the *wake* in the director distortion could extend farther than the computational segment. Moreover, for large pretilts the director distortion also increases in the vicinity of the defect, making its localization less accurate. Conventionally, we identify the region where the energy in the analytical model is larger than the energy in the numerical model as the range of validity of both models: there the latter is generally more accurate than the former.

This, however, should not be mistaken as a static criterion, since the process we are simulating is a non-equilibrium one. To illustrate this further, we repeated the numerical simulation for several pretilts, but statically; that is, fixing the defect position in the centre of the tube segment and searching for an equilibrium solution. The minimum elastic free energy is indeed smaller than the one carried by the moving defect (see figure 5), certainly up to $\varphi_0 \approx 50°$. Figure 6 shows the velocity of the defect delivered by the two models employed here, in the range where they can be compared.

We also studied the dependence of the defect velocity on the elastic anisotropy K_{33}/K_{11} at fixed pretilt angle (see figure 7). When K_{33} is sufficiently large, for instance in the case of pretransitional increase, one expects both escaped structures to become more planar. This yields a larger difference in the energies of the opposite escapes: the driving force then increases as well as the velocity. On the other hand, when K_{33} is sufficiently small ($K_{33} \leqslant 2K_{11}$), the bend deformation, which is dominant

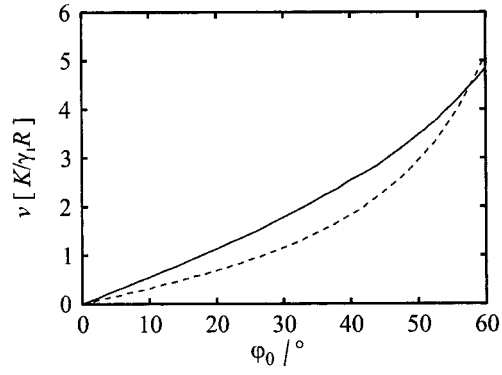

Figure 6. Velocity of a single defect as a function of the pretilt angle φ_0. Solid and dashed lines refer to the numerical and analytical approaches, respectively. Note that the numerical solution is faster than the analytical one up to $\varphi_0 \approx 55°$.

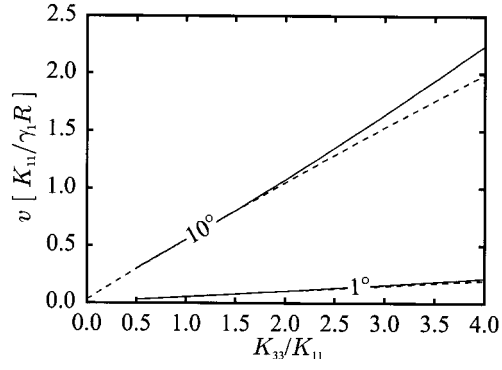

Figure 7. Dependence of the defect velocity on the ratio K_{33}/K_{11} for fixed pretilt (10° and 1°). The solid line represents a radial hedgehog ($s = +1$) and the dashed line a hyperbolic hedgehog ($s = -1$). The velocity is approximately the same for both defects when $K_{33} < 2K_{11}$, whereas the radial hedgehog moves faster than the hyperbolic hedgehog when $K_{33} > 2K_{11}$.

at the tube wall, becomes less expensive, and even appreciable pretilts could only produce small differences in the energies of the opposite escapes. While studying the influence of the K_{33}/K_{11} ratio on the defect velocity, differences in the behaviour of a $+1$ and a -1 defect arose. For large values of the ratio K_{33}/K_{11}, the radial hedgehog ($s=+1$) moves faster than the hyperbolic one ($s=-1$), although the difference in speed is not very large.

We conclude this section with a few quantitative remarks. Experimentally observed velocities of two defects approaching each other at distances $d \gg R$ in a tube with radius 75 μm filled with MBBA are about 0.1 μm min^{-1} [22]. At such distances the velocity cannot be due to interactions between the defects, but is rather a consequence of slight deviations from the homeotropic anchoring at the tube wall. Taking $K_{ii} = 7 \times 10^{-12}$ N, $\gamma_1 = 0.077$ Pa s for MBBA (see Chap. 5 of [10]), a pretilt $\varphi_0 \sim 1°$ is enough to explain the observed velocity. Similar values are obtained for 5CB in a tube with radii 150 and 200 μm [9]. The velocity is proportional to $1/R$, and so small pretilts of the order of 1° can result in velocities observable in small tubes, whereas in larger tubes a defect may be *locked* by irregularities on the wall.

5. Conclusions

We have studied numerically the motion of a single point defect in a cylindrical capillary with tilted anchoring, improving an existing analytical model which employs a family of constrained director fields. This is indeed the main limitation of that model: it overestimates the dissipation in the system, thus predicting a smaller velocity for the defect. The numerical model adopted here is better suited to non-equilibrium situations, though it may still fail to be accurate for large values of the boundary pretilt. By comparing the analytical and the numerical models we have developed a criterion to identify the range of validity of both.

In summary, by comparing the results of both methods we can show that the behaviour of a single point defect in a tube with tilted anchoring generally exhibits two regimes. For small pretilts (up to 20°) the velocity depends almost linearly on the pretilt, whereas for large pretilts (greater than 40°) the velocity increases significantly faster than the pretilt. The latter regime, however, cannot be extended much farther (above 50°), because both approaches become unreliable for large pretilts.

Our study resulted from combining two methods that complement each other. Its outcomes suggest that other problems could also profit from a similar interplay between analytical and numerical approaches, especially the aspects of the dynamics of a single defect set aside here, such as the role of backflow and the ability of an electric or magnetic field applied along the axis of the tube to stop a moving defect, as predicted in [6]. More generally, it would be desirable to extend the methods illustrated in this paper to the annihilation of two point defects with opposite topological charges either in a confining cavity, such as a capillary tube, or in the deep bulk.

This work was supported by the Ministry of Science and Technology of Slovenia (Grant No. J1-0595) and the European Community (SILC TMR ERBFMRX-CT98-0209).

References

[1] Billeter, J. L., Smondyrev, A. M., Loriot, G. B., and Pelcovits, R. A., 1999, *Phys. Rev. E*, **60,** 6831.
[2] Pargelis, A., Turok, N., and Yurke, B., 1991, *Phys. Rev. Lett.*, **67,** 1570.
[3] Minoura, K., Kimura, Y., Ito, K., Hayakawa, R., and Miura, T., 1998, *Phys. Rev. E*, **58,** 643.
[4] Lavrentovich, O. D., and Rozhkov, S. S., 1988, *Pis'ma Zh. eksp. teor. Fiz.*, **47,** 210 [1988, *JETP Lett.*, **47,** 254].
[5] Cladis, P. E., and Brand, H. R., 2000, personal communication.
[6] Guidone Peroli, G., Hillig, G., Saupe, A., and Virga, E. G., 1998, *Phys. Rev. E*, **58,** 3259.
[7] Guidone Peroli, G., and Virga, E. G., 1999, *Phys. Rev. E*, **59,** 3027.
[8] Crawford, G. P., Allender, D. W., and Doane, J. W., 1992, *Phys. Rev. A*, **45,** 8693.
[9] Saupe, A., and Hillig, G., 1998, personal communication.
[10] De Gennes, P. G., and Prost, J., 1993, *The Physics of Liquid Crystals* (Oxford: Clarendon Press).
[11] Cladis, P. E., and Klèman, M., 1972, *J. Phys. (Paris)*, **33,** 591.
[12] Meyer, R. B., 1973, *Phil. Mag.*, **77,** 405.
[13] Ericksen, J. L., 1961, *Trans. Soc. Rheol.*, **5,** 23.
[14] Leslie, F. M., 1968, *Arch. Rat. Mech. Anal.*, **28,** 265.
[15] Landau, L. D., and Khalatnikov, I. M., 1954, *Dokl. Akad. nauk SSSR*, **96,** 469.
[16] Sonnet, A. M., 2001, personal communication.
[17] Leslie, F. M., 1992, *Continuum Mech. Thermodyn.*, **4,** 167.
[18] Sonnet, A. M., and Virga, E. G., 2001, *Phys. Rev. E.*, **64,** 31 705.
[19] Guidone Peroli, G., and Virga, E. G., 1997, *IMA J. appl. Math.*, **58,** 211.
[20] Guidone Peroli, G., and Virga, E. G., 1999, *Comm. math. Phys.*, **200,** 195.
[21] Pismen, L. M., and Rubinstein, B. Y., 1992, *Phys. Rev. Lett.*, **69,** 96.
[22] Ericksen, J. L., 1996, in *Nonlinear Effects in Fluids and Solids*, edited by M. M. Carroll and M Hayes (New York: Plenum Press), 137.